



## *Ab initio* prediction of ordered ground-state structures in $\text{ZrO}_2\text{-Y}_2\text{O}_3$

A. Predith,<sup>1</sup> G. Ceder,<sup>1</sup> C. Wolverton,<sup>2</sup> K. Persson,<sup>1</sup> and T. Mueller<sup>1</sup>

<sup>1</sup>*Department of Materials Science and Engineering, Massachusetts Institute of Technology, 77 Massachusetts Avenue, Cambridge, Massachusetts 02139, USA*

<sup>2</sup>*Department of Materials Science and Engineering, Northwestern University, 2220 Campus Drive, Evanston, Illinois, 60208-3108, USA*

(Received 6 January 2008; published 4 April 2008)

A coupled cluster expansion was used to direct an *ab initio* search for stable ordered structures on the cubic fluorite lattice across the  $\text{ZrO}_2\text{-Y}_2\text{O}_3$  composition range. The energies of 453 arrangements of (Zr, Y) cations and (O, vacancy) anions on the fluorite lattice were calculated by using density functional theory (DFT) in the generalized gradient approximation. These DFT energies were used to construct a coupled cluster expansion that allowed the search for possible  $T=0$  K ground-state structures through  $\sim 10^5$  cation/anion configurations. Our approach correctly identifies the experimentally observed compound  $\text{Zr}_3\text{Y}_4\text{O}_{12}$  and also predicts an as-yet-unobserved ordered structure with  $\text{Zr}_4\text{Y}_2\text{O}_{11}$  stoichiometry. In the latter structure, vacancies are at second nearest neighbors from yttrium and every Zr has seven oxygen first nearest neighbors. The Zr-O bond lengths and oxygen coordination around Zr in the  $\text{Zr}_4\text{Y}_2\text{O}_{11}$  ground state are nearly the same as those in monoclinic  $\text{ZrO}_2$ . We also predict structures at  $\text{Zr}_5\text{Y}_2\text{O}_{13}$  and  $\text{Zr}_6\text{Y}_2\text{O}_{15}$  that are stable with respect to cubic  $\text{ZrO}_2$  but metastable with respect to monoclinic  $\text{ZrO}_2$ .

DOI: [10.1103/PhysRevB.77.144104](https://doi.org/10.1103/PhysRevB.77.144104)

PACS number(s): 64.60.Cn, 81.30.Dz, 71.15.Mb, 82.45.Xy

### I. INTRODUCTION

Zirconia doped with yttria is a common oxygen ion conductor used in oxygen gas sensors and solid oxide fuel cell electrolytes. However, oxygen conductivity in a  $\text{ZrO}_2\text{-Y}_2\text{O}_3$  system displays an unexpected behavior as yttria is added to zirconia. The introduction of yttria creates charge compensating oxygen vacancies that become mobile at high temperatures. Conductivity increases with yttria addition and peaks at 15%–18%  $\text{YO}_{1.5}$  composition, and then it decreases with the addition of more yttria, despite the presence of more vacancies that could aid oxygen diffusion.<sup>1</sup> Two mechanisms may cause a decrease in conductivity: more yttria increases the number of randomly distributed high-energy Y-Y pathways, making oxygen diffusion less favorable, and the addition of yttria introduces more vacancies that form ordered arrangements and inhibit the diffusion of oxygen into vacant sites.<sup>2–6</sup> The study of ordering in the  $\text{ZrO}_2\text{-Y}_2\text{O}_3$  system is, thus, a subject that has generated much interest. To determine the plausibility of vacancy ordering as an inhibitor of oxygen migration, we perform a computational search for all cation and anion ordered ground-state arrangements across the composition range of  $\text{ZrO}_2\text{-Y}_2\text{O}_3$ . We begin by describing the yttria stabilized zirconia (YSZ) structure, the evidence for short-range ordering, and the driving forces for stability to provide the background of the investigation.

YSZ is a solid solution on a cubic fluorite lattice with yttrium and zirconium on a face-centered-cubic cation lattice and oxygen and vacancies on a simple cubic anion lattice (Fig. 1). In the cubic fluorite structure, each cation is in the center of a cube of eight anions and each oxygen ion or oxygen vacancy is in the center of a cation tetrahedron. An oxygen ion diffuses by hopping across an edge of a tetrahedron between two cations. Experimental reports describe both long-range order (LRO) and short-range order (SRO) in the system. The experimentally identified LRO structure is the  $\delta$  structure with  $\text{Zr}_3\text{Y}_4\text{O}_{12}$  stoichiometry.<sup>7</sup> The reported

atomic coordinates of the  $\delta$  structure indicate that vacancies are in  $\langle 1\ 1\ 1 \rangle$  chains along the body diagonals of the anion cubes, with every other cube along the chain having a zirconium in the center.

The ordered  $\delta$  structure is intermediate in composition between pure yttria and pure zirconia, and the ground-state structures of the pure compounds can be described with respect to the fluorite structure. The pure yttria takes the C-type lanthanide structure, which can be considered an oxygen vacancy ordered superstructure of the cubic fluorite lattice. When the structure is superimposed on a cubic fluorite framework, yttrium ions reside in cation sites, oxygen ions fill  $\frac{3}{4}$  of the anion sites, and the remaining anion sites are vacant. Each yttrium, therefore, has six oxygen neighbors and two vacancy neighbors. The vacancies are at face diago-

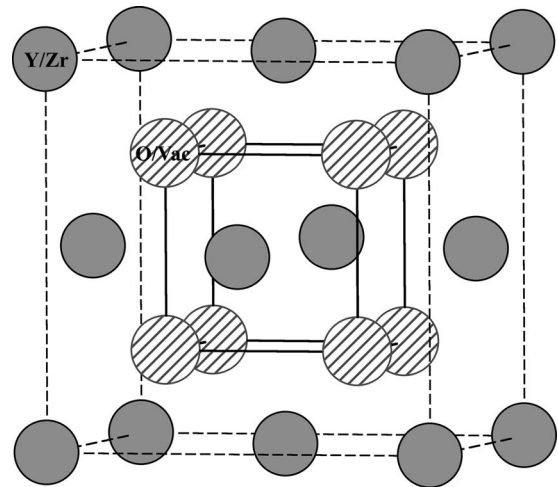


FIG. 1. In the fluorite structure, cations (gray circles, Y/Zr) form a fcc array and anions (striped circles, oxygen/vacancies) form a simple cubic array.

nals in 75% of the anion cubes and at body diagonals in 25% of anion cubes.

In contrast to the cubic basis of yttria, pure zirconia is monoclinic at low temperatures and has Zr in sevenfold coordination by oxygen rather than in eightfold coordination as in a cubic fluorite. The preference for a sevenfold coordination may be due to the small size of the zirconium ion. The radius ratio between oxygen and zirconium is too large to be sixfold coordinated, as dictated by Pauling's rules, but is not large enough to be eightfold coordinated.<sup>8</sup> Doping the larger Y into Zr sites stabilizes the long-range cubic fluorite structure, but local distortions from the cubic structure remain.

While the structures of zirconia, yttria, and the  $\delta$  structure are well documented, the stable atomic structures at intermediate compositions are less clear. The literature gives evidence for SRO of ions and vacancies at low yttria compositions,<sup>7,9-15</sup> but existing phase diagrams of  $\text{ZrO}_2\text{-Y}_2\text{O}_3$  do not contain any ordered structures at compositions less than 57%  $\text{YO}_{1.5}$ .<sup>16</sup> The question remains as to whether or not short-range ordering in the solid solution could also be a fingerprint of as-yet-unobserved LRO compounds. The neutron and x-ray diffraction study of Goff *et al.*<sup>9</sup> describes three types of defects in single crystals: isolated vacancies, divacancy pairs along the body diagonal of an anion cube centered around a cation, and aggregates of the divacancy pairs aligned along  $\langle 1\ 1\ 2 \rangle$ . Another important feature of the atomic arrangements is the relative position of yttrium to oxygen vacancies in the solid solution. Experimental studies observe that in dilute yttria compositions, vacancies reside in the first nearest neighbor position to zirconium.<sup>17,18</sup> Computational studies confirm the tendency of vacancy preference for nearest neighbor sites to Zr.<sup>7,19,20</sup>

In addition to the above reports of LRO and SRO in YSZ, other reports of ordering exist as well: A selected area diffraction study of a material with 50%  $\text{YO}_{1.5}$  shows weak satellite reflections, suggesting ordering features of both C-type yttria and distorted pyrochlore.<sup>11</sup> Other electron diffraction studies of 39% and 48%  $\text{YO}_{1.5}$  single crystals found that the diffuse intensity in the patterns of these crystals resembles the  $\delta$  structure.<sup>12,13</sup>

While some reports in the literature have focused on the structures of YSZ and on the evidence for SRO, others have focused on elucidating the driving forces for stability. One can consider three major driving forces for stability in the system: (1) the electrostatic interaction of ions and vacancies, (2) the preference for sevenfold coordinated zirconium, and (3) the relaxation of ions away from idealized cubic fluorite sites driven by vacancy relaxation and by the size difference between  $\text{Y}^{3+}$  and  $\text{Zr}^{4+}$ .<sup>21</sup>

The effect of relaxation has been extensively discussed. Numerous experimental studies have measured the direction of relaxation of oxygen, Zr, and Y away from cubic fluorite sites.<sup>17,19,22-26</sup> Frey *et al.*<sup>14</sup> offered a thorough review. Computational studies of ordered structures show that the elastic and electrostatic interactions push the structure in opposite directions.<sup>21,27</sup> The elastic component of the energy tends to move the ions away from cubic fluorite sites. Zacate *et al.*,<sup>20</sup> in particular, found in their computational study that oxygen ions relax toward a vacancy when a dopant cation smaller

than Zr is a first nearest neighbor to the vacancy. If the dopant at the first nearest neighbor position is larger than Zr (Y, for example), only some of the oxygen ions relax in position. However, if the dopant larger than Zr is second nearest neighbor to the vacancy, all oxygen ions relax toward the vacancy and the dopant-vacancy pair has the highest binding energy in this configuration.

Given an understanding of the parent YSZ structure, the evidence for SRO, and knowledge of factors driving phase stability, we completed a systematic computational search for ground-state structures. In searching for stable ordered structures, we sought to determine whether experimental reports of SRO are indicative of thermodynamically stable LRO and, if so, to compare the known driving forces for stability in YSZ to the evidence for long-range-ordered structures. Vacancy ordering at low yttria compositions would inhibit oxygen conductivity and explain why oxygen conductivity in YSZ peaks and decreases with increasing yttrium and vacancy concentration.

## II. METHODS

Several approaches to searching for low-energy structures in materials exist. Some of these methods involve searching through crystallographic databases by either using brute force<sup>28-30</sup> or using data mining approaches.<sup>31,32</sup> These methods have been quite effective in a number of applications, but they have the serious restriction of being incapable of predicting completely unobserved crystal structure types. Besides these methods, however, there are those that do not have the said restriction and are capable of predicting new structure types: genetic algorithm methods,<sup>33</sup> lattice algebra enumeration methods,<sup>34</sup> and cluster expansion techniques. For problems in which one desires to find low-energy configurations of atoms or ions on a fixed lattice topology, the cluster expansion is the most mature and effective computational tool. A cluster expansion is essentially a parametrization of the total energy in terms of variables that describe the occupation of each lattice site<sup>35-38</sup> and has been applied to a wide variety of alloys, including metallic,<sup>37-39</sup> semiconductor,<sup>38,40</sup> and oxide<sup>41,42</sup> systems. It has also been applied to the modeling of phase diagrams,<sup>37,38</sup> short-range order,<sup>43</sup> vibrational entropies,<sup>44</sup> and equilibrium and kinetic evolution of precipitates.<sup>45-47</sup>

Cluster expansions are commonly used to model systems with a binary disorder (i.e., two species can occupy the sites of a lattice). The YSZ system is more complex than a simple binary system because it contains a binary disorder on both cation (Y-Zr) and anion (oxygen-vacancy) sublattices. To deal with materials that have a disorder on multiple sublattices, Tepeš developed the coupled cluster expansion (CCE) approach.<sup>48</sup>

In a typical simple binary cluster expansion, a spin variable  $\sigma_i$  with a value of +1 or -1 denotes the type of atom sitting on each site  $i$ . One then expands the energy (or any other function of configuration) in polynomials of the discrete variables  $\sigma_i$ . The polynomials called *cluster functions* are the product of the spin variables at one or more sites and form a complete orthonormal basis.<sup>35</sup> In a coupled cluster

expansion, two lattices can be simultaneously considered with a different set of spin variables for each of the two sublattices ( $\sigma, \theta$ ). Cluster functions are then defined with products of spin variables from either or both sublattices,

$$E(\sigma, \theta) = V_o + \sum_i V_i \sigma_i + \sum_i V_i \theta_i + \sum_{i,j} V_{i,j} \sigma_i \sigma_j + \sum_{i,j} V_{i,j} \sigma_i \theta_j + \sum_{i,j} V_{i,j} \theta_i \theta_j + \sum_{i,j,k} V_{i,j,k} \sigma_i \sigma_j \theta_k + \sum_{i,j,k} V_{i,j,k} \sigma_i \theta_j \theta_k \dots \quad (1)$$

Such product basis is mathematically complete and has been used to model complex chemical systems.<sup>48</sup>

In YSZ, two lattices must be considered: cations approximately sit on fcc lattice sites and anions sit on simple cubic lattice sites. The set of clusters of the YSZ expansion includes clusters with only anion sites, clusters with only cation sites, and clusters with both anion and cation sites and, as such, includes anion-anion, cation-cation, and anion-cation interactions. The effective cluster interactions (ECIs) can be determined by fitting Eq. (1) with the calculated energy of a large number of ordered arrangements of  $\text{ZrO}_2\text{-Y}_2\text{O}_3$ . For each structure, the occupation variables  $\sigma_i$  and  $\theta_j$  in Eq. (1) may be evaluated from the unit cells.

In a matrix notation, the cluster expansion becomes a mathematical fit solved by least-squares minimization or linear programming routines,<sup>49,50</sup>

$$\mathbf{E}_m = \mathbf{X}_{m \times n} \mathbf{V}_n, \quad (2)$$

where  $\mathbf{E}_m$  is a vector of  $m$  structural energies,  $\mathbf{X}_{m \times n}$  is a matrix containing the values of the  $n$  cluster functions evaluated in all  $m$  structures, and  $\mathbf{V}_n$  are the ECIs to be determined. In this paper, the energy for a configuration of cations ( $\sigma$ ) or anions ( $\theta$ ) is expressed as the formation energy of a structure per cation, which is simply the total energy of the configuration minus the composition-weighted average of the energies of pure zirconia and pure yttria,

$$E_{\text{formation}}(\sigma, \theta) = E_{\text{per cation}}(\sigma, \theta) - x_{\text{YO}_{1.5}} E_{\text{YO}_{1.5}} - (1 - x_{\text{YO}_{1.5}}) E_{\text{ZrO}_2}. \quad (3)$$

The formation energies may be defined with respect to either the monoclinic  $\text{ZrO}_2$  energy or the cubic  $\text{ZrO}_2$  energy. The ground states are the structures that form the lowest convex hull in the  $E_{\text{formation}}\text{-}x_{\text{YO}_{1.5}}$  space ensuring that the ground states or their linear combination are below the energy of any other structure.

Once the ECIs are known, one can rapidly determine the energetics for any configuration of ions. A quick evaluation of energies is essential to finding ground states amid a large number of potential structures. To search for ground states in YSZ, we enumerated a database of all structures that are possible in supercells of nine primitive fcc unit cells or smaller. Each primitive unit cell has one cation and two anion sites, and the database forms our population of 81 827 “trial” ground-state structures. Starting with a set of energies calculated with density functional theory in the generalized gradient approximation, we search for ground-state structures by following an iterative approach.

(1) Step 1: Determine the ECI by fitting to calculated density functional theory (DFT) energies of structures.

(2) Step 2: By using the ECI, obtain estimated energies for the complete set of 81 827 trial structures and construct a convex hull.

(3) Step 3: For the trial structures with low estimated energies (energies near or below the convex hull), calculate the DFT energy (if not already in the DFT set).

(4) Step 4: If both CCE and DFT consistently give the same stability of low-energy structures (same structures on the convex hull), stop. Otherwise, return to step 1 with a new DFT set and refit the ECI.

This procedure tends to converge to a stable set of ground-state structures. The errors in the energies predicted by the cluster expansion relative to the direct DFT-calculated energies decrease with each iteration as more energies are added to the expansion, and the structures predicted to be at or below the convex hull are more frequently confirmed so by the direct DFT calculation. Binary cluster expansions typically show convergence with approximately 10–50 DFT energies; however, we found that the complexity of the coupled cluster expansion makes quantitative convergence more difficult to achieve. By using an initial database of 120 DFT energies, we constructed the coupled cluster expansion of YSZ and added DFT energies to converge the cluster expansion. As energies were added, we also implemented the iterative process to identify the ground-state structures of the system. The final database contained 453 DFT energies, representing a very large database of DFT energies for this system.

The DFT total energies of each structure used to fit the cluster expansion are obtained by using the Vienna *ab initio* simulation package<sup>51,52</sup> (VASP) within the generalized gradient approximation using the PW91 exchange-correlation functional.<sup>53–55</sup> The calculations use ultrasoft pseudopotentials<sup>56</sup> and a plane-wave basis set with an energy cutoff of 515 eV. Starting with configurations of ions in exact cubic fluorite positions, the ion positions and unit cell volumes are allowed to relax during energy minimization whereby the Brillouin zone is sampled with a  $2 \times 2 \times 2$   $k$ -point mesh. A second relaxation on a  $4 \times 4 \times 4$   $k$ -point mesh gives the final energy. Calculations of some structures with a  $6 \times 6 \times 6$   $k$ -point mesh ensured that the  $4 \times 4 \times 4$   $k$ -point mesh was adequate for a  $k$ -point convergence.

### III. RESULTS AND DISCUSSION

The development of the cluster expansion and the iterative search for ground states led to the direct DFT calculation of 453 structures across the compositions 0%, 22%, 25%, 29%, 33%, 44%, 50%, 57%, 67%, 73%, 75%, 80%, 86%, 89%, and 100%  $\text{YO}_{1.5}$ . The energies of the structures with respect to monoclinic  $\text{ZrO}_2$  and  $C$ -type yttria are shown in Fig. 2. By evaluating the energies of 81 827 trial structures of both common and unusual structure types, the cluster expansion finds two ground-state stable structures that lie on the convex hull:  $\text{Zr}_4\text{Y}_2\text{O}_{11}$  (with 33%  $\text{YO}_{1.5}$  composition) and  $\text{Zr}_3\text{Y}_4\text{O}_{12}$  (with 57%  $\text{YO}_{1.5}$  composition). The cluster

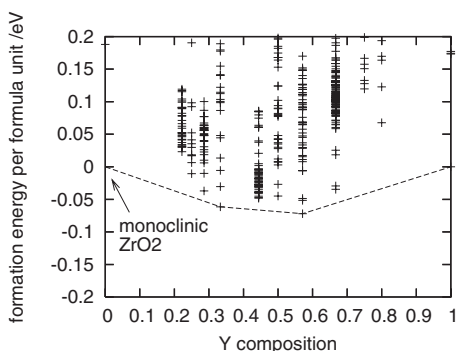


FIG. 2. The convex hull of DFT energies with monoclinic  $ZrO_2$  and C-type  $YO_{1.5}$  as end members shows structures at 33% Y ( $Zr_4Y_2O_{11}$ ) and 57% Y ( $Zr_3Y_4O_{12}$ ) as the ground states. Only structures with formation energies of up to 0.2 eV are shown.

expansion successfully finds the experimentally identified  $\delta$  structure<sup>7</sup> as the  $Zr_3Y_4O_{12}$  ground state. The  $Zr_4Y_2O_{11}$  structure is predicted by the cluster expansion and confirmed with DFT calculations. The primitive unit cell is in Table I, and the discussion of the  $Zr_4Y_2O_{11}$  structure below details its unique features.

The *monoclinic* structure is the true low-temperature ground-state phase of zirconia, but plotting the formation energies of the 453 structures with respect to the formation energies of *cubic*  $ZrO_2$  and C-type yttria gives insight into metastable structures that may be present in the YSZ system. Cubic  $ZrO_2$  is dynamically unstable, and previous work addresses the instability of  $ZrO_2$ .<sup>57,58</sup> Here, we consider only zero temperature and static energies, without explicitly con-

TABLE I. The table gives the primitive unit cell of the ground-state  $Zr_4Y_2O_{11}$  and its atomic positions in fractional coordinates.

$\vec{a}=6.422 \text{ \AA}$		$\alpha=116^\circ$	
$\vec{b}=6.422 \text{ \AA}$		$\beta=116^\circ$	
$\vec{c}=12.36 \text{ \AA}$		$\gamma=120^\circ$	
0.813	0.153	0.493	Y
0.487	0.480	0.493	Y
0.954	0.994	0.995	Zr
0.681	0.348	0.991	Zr
0.327	0.620	0.995	Zr
0.216	0.883	0.526	Zr
0.493	0.868	0.921	O
0.201	0.160	0.921	O
0.854	0.520	0.892	O
0.202	0.869	0.347	O
0.889	0.274	0.333	O
0.608	0.556	0.333	O
0.383	0.403	0.640	O
0.084	0.751	0.640	O
0.736	0.049	0.640	O
0.179	0.518	0.108	O
0.851	0.845	0.108	O

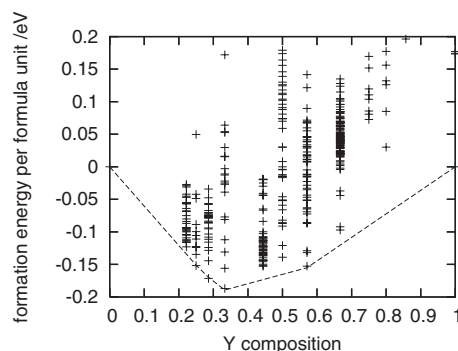


FIG. 3. The convex hull of DFT energies with cubic  $ZrO_2$  and C-type  $YO_{1.5}$  as end members shows ground-state structures at 25% Y ( $Zr_6Y_2O_{15}$ ), 29% Y ( $Zr_5Y_2O_{13}$ ), 33% Y ( $Zr_4Y_2O_{11}$ ), and 57% Y ( $Zr_3Y_4O_{12}$ ). Only structures with formation energies of up to 0.2 eV are shown.

sidering destabilizing phonons in the calculations. Upon the experimental addition of yttria to zirconia, the system becomes stabilized in a cubic fluorite solid solution.

A plot of the formation energies with respect to cubic  $ZrO_2$  is presented in Fig. 3. Four ground states lie on the convex hull. The two ground states of the monoclinic hull as well as two additional structures— $Zr_5Y_2O_{13}$  (with 29%  $YO_{1.5}$  composition) and  $Zr_6Y_2O_{15}$  (with 25%  $YO_{1.5}$  composition)—are present. The primitive unit cells of the two new cubic ground states are given in Table II. While they may not be present at low temperatures in competition with monoclinic  $ZrO_2$ , the  $Zr_6Y_2O_{15}$  and  $Zr_5Y_2O_{13}$  structures are locally stable on the cubic fluorite lattice, and a short-range order in the real system may be indicative of these structures.

We give coordinates for all predicted stable and metastable low-energy ordered states on the cubic fluorite lattice but discuss only the  $Zr_4Y_2O_{11}$  structure in more detail. It represents a true  $T=0$  K ground state within DFT (with respect to monoclinic  $ZrO_2$ ). The observed  $\delta$  phase has been previously discussed in some detail.

A long-range ordered structure has not been previously confirmed in  $Zr_4Y_2O_{11}$ , but the ground state in this composition has interesting ordering features. The symmetry of the predicted  $Zr_4Y_2O_{11}$  structure is  $C2/m$ . The (1 1 1) cation planes alternate between pure Zr planes and mixed Y and Zr planes. The mixed planes contain Zr surrounded by hexagons of Y (Fig. 4); hence, Y and Zr in the mixed planes form a common and stable pattern on the triangular lattice.<sup>59</sup> Oxygen vacancies are first nearest neighbors to all Zr and second nearest neighbors to Y.

Since the ionic arrangement along  $\langle 1 1 2 \rangle$  was previously recognized in YSZ, we also describe  $Zr_4Y_2O_{11}$  from that vantage point.<sup>9</sup> In the mixed planes of Fig. 4, one can identify two Zr  $\langle 1 1 2 \rangle$  chains alternating with a single Y  $\langle 1 1 2 \rangle$  chain. Vacancies form parallel  $\langle 1 1 2 \rangle$  chains in the anion planes, and the vacancies are equally distributed throughout the anion sublattice at sixth nearest neighbors to each other. The vacancy chains are arranged, so they are at second nearest neighbors to yttrium.

The distinctive feature of the  $Zr_4Y_2O_{11}$  predicted structure is that all vacancies are nearest neighbor to zirconium ions

TABLE II. Columns 1–4 contain the fully relaxed unit cell and atom positions in fractional coordinates of the ground-state  $Zr_6Y_2O_{15}$  on the cubic fluorite convex hull. Columns 5–8 contain the fully relaxed unit cell and atom positions in fractional coordinates of the ground-state  $Zr_5Y_2O_{13}$  on the cubic fluorite convex hull.

$\vec{a}=6.398 \text{ \AA}$				$\vec{a}=6.513 \text{ \AA}$			
$\vec{b}=15.217 \text{ \AA}$				$\vec{b}=6.341 \text{ \AA}$			
$\vec{c}=16.029 \text{ \AA}$				$\vec{c}=6.419 \text{ \AA}$			
$\alpha=88.1^\circ$				$\alpha=99.9^\circ$			
$\beta=66.4^\circ$				$\beta=101^\circ$			
$\gamma=24.5^\circ$				$\gamma=99.1^\circ$			
0.607	0.005	0.879	Y	0.998	0.983	0.011	Y
0.268	0.040	0.136	Y	0.428	0.709	0.835	Y
0.168	0.938	0.972	Zr	0.855	0.432	0.750	Zr
0.589	0.956	0.496	Zr	0.242	0.141	0.580	Zr
0.166	0.999	0.374	Zr	0.710	0.899	0.427	Zr
0.168	0.026	0.766	Zr	0.185	0.570	0.285	Zr
0.787	0.986	0.234	Zr	0.554	0.263	0.119	Zr
0.836	0.008	0.633	Zr	0.760	0.722	0.699	O
0.665	0.935	0.350	O	0.132	0.471	0.578	O
0.827	0.670	0.742	O	0.676	0.232	0.441	O
0.353	0.678	0.636	O	0.009	0.852	0.352	O
0.492	0.828	0.197	O	0.504	0.589	0.215	O
0.430	0.714	0.017	O	0.878	0.361	0.078	O
0.110	0.663	0.515	O	0.311	0.038	0.885	O
0.294	0.816	0.407	O	0.260	0.237	0.268	O
0.992	0.738	0.901	O	0.669	0.954	0.098	O
0.381	0.208	0.822	O	0.127	0.661	0.980	O
0.633	0.314	0.361	O	0.522	0.367	0.794	O
0.348	0.263	0.213	O	0.957	0.121	0.698	O
0.928	0.242	0.720	O	0.402	0.862	0.513	O
0.752	0.157	0.574	O				
0.989	0.288	0.101	O				
0.560	0.277	0.985	O				

(a)

(b)

and that all Zr have one first nearest neighbor vacancy, making all Zr sevenfold coordinated by oxygen (Fig. 5). By calculating how yttria doping affects zirconium coordination at different concentrations, Ho<sup>60</sup> postulated that a structure with all Zr in sevenfold coordination by oxygen would be stable. The stability of  $Zr_4Y_2O_{11}$  can be rationalized as an optimal solution to several competing energetic factors: (1) *size effects*: Zr ions can be sevenfold coordinated, as in pure  $ZrO_2$ , (2) *cation ordering*: Y and Zr are arranged on the cation sublattice in a common low-energy configuration for a triangular lattice, and (3) *electrostatic repulsion*: the oxygen vacancies are maximally separated on the cubic sublattice.

The bond lengths further reflect the low energy of this structure. In cubic  $ZrO_2$ , the calculated Zr-O first nearest neighbor bond length is 2.29 Å, and each of the four Zr in the monoclinic zirconia structure has an average Zr-O bond length of 2.19 Å. The four Zr in  $Zr_4Y_2O_{11}$  have average Zr-O bond lengths of 2.18, 2.19, 2.19, and 2.21 Å, which are very close to the bond lengths in monoclinic  $ZrO_2$ . The average Y-O bond lengths for the two Y ions in the ground state are both 2.43 Å, while the average Y-O bond length for all 16 Y ions of the C-type yttria structure is 2.32 Å. The character of the Zr-O bond in pure  $ZrO_2$  has been under investigation,

and the covalency in the Zr-O bond may be necessary to accurately model zirconia polymorphs.<sup>58</sup> The degree of covalency may have implications for bonding in both pure and doped zirconias.

#### IV. CONCLUSIONS

This study used a coupled cluster expansion together with density functional theory calculations to examine ordered structures across the  $ZrO_2$ - $Y_2O_3$  composition range. A database of 81 827 cation and anion ordered arrangements was developed with all possible YSZ structures on the cubic fluorite lattice with supercells containing nine or fewer primitive unit cells.

By using the coupled cluster expansion to suggest possible ground-state structures from the database, we iteratively calculated the suggested structures with DFT and reparameterized the cluster expansion. The development of the cluster expansion and the iterative process led to the calculation of DFT formation energies for 453 structures and identified four ordered ground states at compositions between cubic zirconia and C-type yttria.

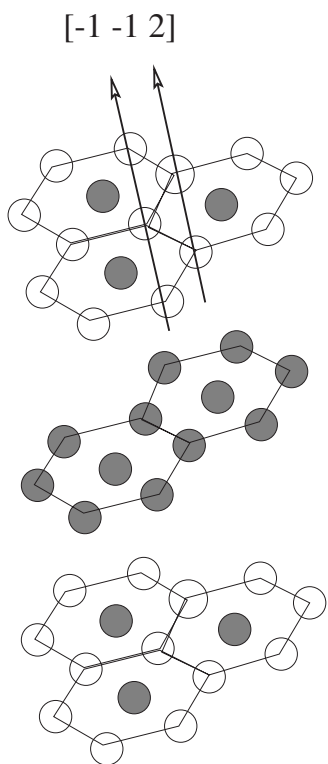


FIG. 4. (1 1 1) cation planes in cubic YSZ appear hexagonal. In the  $Zr_4Y_2O_{11}$  ground state, every other cation plane is all Zr (filled circles). The alternating plane is  $\frac{2}{3}$  Y (open circles) and  $\frac{1}{3}$  Zr. The arrows indicate the  $[-1 -1 2]$  direction along the face of the (1 1 1) plane.

The ground-state  $Zr_4Y_2O_{11}$  is a previously unidentified phase and is stable with respect to monoclinic zirconia and the  $\delta$  structure  $Zr_3Y_4O_{12}$ . The  $Zr_4Y_2O_{11}$  structure contains hallmarks of stability found in YSZ: yttrium and vacancies at second nearest neighbors, relaxation of Zr-O bond lengths, and sevenfold coordination of zirconium by oxygen as in monoclinic  $ZrO_2$ . The peak in oxygen ionic conductivity in the zirconia-yttria system is at 15%–18%  $YO_{1.5}$  composition. The discovery of metastable ordered structures at 25% and

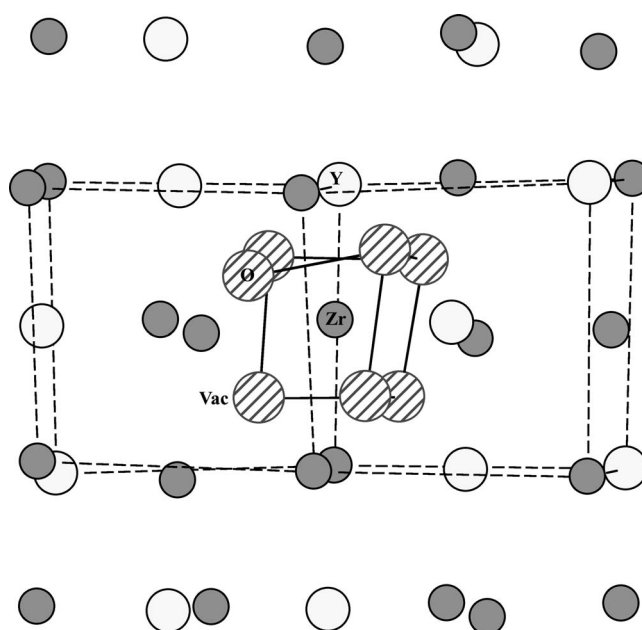


FIG. 5. Each zirconium (filled circle) in the  $Zr_4Y_2O_{11}$  ground state is coordinated by seven oxygens (striped circles). The open circles are yttrium. If the structure is mapped onto a fluorite structure, the dotted lines indicate a fcc cation array and “Vac” denotes the approximate position of a vacant anion site.

29%  $YO_{1.5}$  and a ground state at 33%  $YO_{1.5}$  suggests that a short-range order at these compositions may be expected at nonzero temperatures. This short-range order may be responsible for the observed decline in ionic conductivity at these compositions.

### ACKNOWLEDGMENTS

The authors acknowledge funding from the Ford Motor Co. and the Department of Energy and useful discussions with A. Bogicevic. A.P. acknowledges useful discussions with A. Van der Ven.

<sup>1</sup>T. Etsell and S. Flengas, *Chem. Rev.* (Washington, D.C.) **70**, 339 (1970).  
<sup>2</sup>M. Khan, M. Islam, and D. Bates, *J. Mater. Chem.* **8**, 2299 (1998).  
<sup>3</sup>M. Kilo, R. Jackson, and G. Borshardt, *Philos. Mag.* **83**, 3309 (2003).  
<sup>4</sup>V. Zavodinsky, *Phys. Solid State* **46**, 453 (2004).  
<sup>5</sup>R. Krishnamurthy, Y. Yoon, D. Srolovitz, and R. Car, *J. Am. Ceram. Soc.* **87**, 1821 (2004).  
<sup>6</sup>M. Martin, *Z. Phys. Chem.* **219**, 105 (2005).  
<sup>7</sup>A. Bogicevic, C. Wolverton, G. Crosbie, and E. Stechel, *Phys. Rev. B* **64**, 014106 (2001).  
<sup>8</sup>W. Kingery, H. Bowen, and D. Uhlmann, *Introduction to Ceramics*, 2nd ed. (Wiley, New York, 1976).

<sup>9</sup>J. P. Goff, W. Hayes, S. Hull, M. T. Hutchings, and K. N. Clausen, *Phys. Rev. B* **59**, 14202 (1999).  
<sup>10</sup>M. Morinaga and J. B. Cohen, *Acta Crystallogr., Sect. A: Cryst. Phys., Diffr., Theor. Gen. Crystallogr.* **36**, 520 (1980).  
<sup>11</sup>J. Irvine, A. Feighery, D. Fagg, and S. Garcia-Martin, *Solid State Ionics* **136-137**, 879 (2000).  
<sup>12</sup>A. Gallardo-Lopez, J. Martinez-Fernandez, and A. Dominguez-Rodriguez, *Philos. Mag. A* **81**, 1675 (2001).  
<sup>13</sup>A. Gallardo-Lopez, J. Martinez-Fernandez, and A. Dominguez-Rodriguez, *J. Eur. Ceram. Soc.* **22**, 2821 (2002).  
<sup>14</sup>F. Frey, H. Boysen, and I. Kaiser-Bischoff, *Z. Kristallogr.* **220**, 1017 (2005).  
<sup>15</sup>M. Fèvre, A. Finel, and R. Caudron, *Phys. Rev. B* **72**, 104117 (2005).

- <sup>16</sup> *Phase Diagrams for Zirconium and Zirconia Systems*, edited by H. Ondik and H. McMurdie (American Ceramic Society, Westerville, OH, 1998).
- <sup>17</sup> C. Catlow, A. Chadwick, G. N. Greaves, and L. Moroney, *J. Am. Ceram. Soc.* **69**, 272 (1986).
- <sup>18</sup> P. Li, I. Chen, and J. Penner-Hahn, *J. Am. Ceram. Soc.* **77**, 118 (1994).
- <sup>19</sup> G. Stapper, M. Bernasconi, N. Nicoloso, and M. Parrinello, *Phys. Rev. B* **59**, 797 (1999).
- <sup>20</sup> M. Zacate, L. Minervini, D. Bradfield, R. Grimes, and K. Sickafus, *Solid State Ionics* **128**, 243 (2000).
- <sup>21</sup> A. Bogicevic and C. Wolverton, *Phys. Rev. B* **67**, 024106 (2003).
- <sup>22</sup> D. Steele and B. Fender, *J. Phys. C* **7**, 1 (1974).
- <sup>23</sup> D. Argyriou, M. Elcombe, and A. Larson, *J. Phys. Chem. Solids* **57**, 183 (1996).
- <sup>24</sup> K. McClellan, S.-Q. Xiao, K. Lagerlof, and A. Heuer, *Philos. Mag. A* **70**, 185 (1994).
- <sup>25</sup> S. Suzuki, M. Tanaka, and M. Ishigame, *J. Phys. C* **20**, 2963 (1987).
- <sup>26</sup> T. Welberry, R. Withers, J. Thompson, and B. Butler, *J. Solid State Chem.* **100**, 71 (1992).
- <sup>27</sup> A. Bogicevic and C. Wolverton, *Europhys. Lett.* **56**, 393 (2001).
- <sup>28</sup> O. M. Løvvik and O. Swang, *Europhys. Lett.* **67**, 607 (2004).
- <sup>29</sup> P. Va Jeeston, P. Ravindran, A. Kjekshus, and H. Fjellvg, *J. Alloys Compd.* **363**, L7 (2004).
- <sup>30</sup> C. Wolverton and V. Ozoliņš, *Phys. Rev. B* **75**, 064101 (2007).
- <sup>31</sup> S. Curtarolo, D. Morgan, K. Persson, J. Rodgers, and G. Ceder, *Phys. Rev. Lett.* **91**, 135503 (2003).
- <sup>32</sup> C. Fischer, K. Tibbetts, D. Morgan, and G. Ceder, *Nat. Mater.* **5**, 641 (2006).
- <sup>33</sup> A. R. Oganov and C. W. Glass, *J. Chem. Phys.* **124**, 244704 (2006).
- <sup>34</sup> B. Magyari-Köpe, V. Ozoliņš, and C. Wolverton, *Phys. Rev. B* **73**, 220101(R) (2006).
- <sup>35</sup> J. Sanchez, F. Ducastelle, and D. Gratias, *Physica A* **128**, 334 (1984).
- <sup>36</sup> J. W. D. Connolly and A. R. Williams, *Phys. Rev. B* **27**, 5169 (1983).
- <sup>37</sup> D. de Fontaine, in *Solid State Physics: Advances in Research and Applications*, edited by Henry Ehrenreich and David Turnbull (Academic, San Diego, 1994), Vol. 47, Chap. 2, pp. 33–176.
- <sup>38</sup> A. Zunger, *First Principles Statistical Mechanics of Semiconductor Alloys and Intermetallic Compounds*, in NATO Advanced Studies Institute on Statics and Dynamics of Alloy Phase Transformations, edited by P. Turchi and A. Gonis, p. 361, (Plenum Press, New York, 1994).
- <sup>39</sup> C. Wolverton and A. Zunger, *Comput. Mater. Sci.* **8**, 107 (1997).
- <sup>40</sup> C. Wolverton and A. Zunger, *Phys. Rev. Lett.* **75**, 3162 (1995).
- <sup>41</sup> B. P. Burton, *Phys. Rev. B* **59**, 6087 (1999).
- <sup>42</sup> A. Van der Ven, M. K. Aydinol, G. Ceder, G. Kresse, and J. Hafner, *Phys. Rev. B* **58**, 2975 (1998).
- <sup>43</sup> C. Wolverton, V. Ozoliņš, and A. Zunger, *J. Phys.: Condens. Matter* **12**, 2749 (2000).
- <sup>44</sup> V. Ozoliņš, C. Wolverton, and A. Zunger, *Phys. Rev. B* **57**, 6427 (1998).
- <sup>45</sup> C. Wolverton, *Philos. Mag. Lett.* **79**, 683 (1999).
- <sup>46</sup> S. Müller, L.-W. Wang, A. Zunger, and C. Wolverton, *Phys. Rev. B* **60**, 16448 (1999).
- <sup>47</sup> J. Wang, C. Wolverton, S. Müller, Z.-K. Liu, and L.-Q. Chen, *Acta Mater.* **53**, 2759 (2005).
- <sup>48</sup> P. Tepeš, Ph.D. thesis, Massachusetts Institute of Technology, 1996.
- <sup>49</sup> S. R. Searle, *Linear Models* (Wiley, New York, 1971).
- <sup>50</sup> D. Bertsimas and J. Tsitsiklis, *Introduction to Linear Optimization* (Athena Scientific, Belmont, 1997).
- <sup>51</sup> G. Kresse and J. Furthmüller, *Phys. Rev. B* **54**, 11169 (1996).
- <sup>52</sup> G. Kresse and J. Furthmüller, *Comput. Mater. Sci.* **6**, 15 (1996).
- <sup>53</sup> P. Hohenberg and W. Kohn, *Phys. Rev.* **136**, B864 (1964).
- <sup>54</sup> W. Kohn and L. Sham, *Phys. Rev.* **140**, A1133 (1965).
- <sup>55</sup> J. Perdew, *Electronic Structure of Solids 1991*, edited by P. Ziesche and H. Eschrig (Akademie, Berlin, 1991), Vol. 11.
- <sup>56</sup> D. Vanderbilt, *Phys. Rev. B* **32**, 8412 (1985).
- <sup>57</sup> M. W. Finnis, A. T. Paxton, M. Methfessel, and M. van Schilf-gaarde, *Phys. Rev. Lett.* **81**, 5149 (1998).
- <sup>58</sup> S. Fabris, A. T. Paxton, and M. W. Finnis, *Phys. Rev. B* **61**, 6617 (2000).
- <sup>59</sup> G. Ceder and A. Van der Ven, *Electrochim. Acta* **45**, 131 (1999).
- <sup>60</sup> S. Ho, *Mater. Sci. Eng.* **54**, 23 (1982).